

Structural, superconducting, and magnetic properties of $\text{YNi}_2\text{B}_2\text{C}$ and $\text{ErNi}_2\text{B}_2\text{C}$

C. Godart*

Centre National de la Recherche Scientifique, UPR 209, Meudon 92195, France

L.C. Gupta, R. Nagarajan, and S.K. Dhar

Tata Institute of Fundamental Research, Homi Bhabha Road, Bombay 400 005, India

H. Noel and M. Potel

CNRS URA 1495, Chimie du Solide et Inorganique Moleculaire, Universite de Rennes 1-35042 Rennes Cedex, France

Chandan Mazumdar

Department of Physics, Indian Institute of Technology, Bombay 400 076, India

Zakir Hossain

Tata Institute of Fundamental Research, Homi Bhabha Road, Bombay 400 005, India

C. Levy-Clement*

Laboratoire Physique Solides, CNRS, Meudon, F-92195, France

G. Schiffmacher

Centre National de la Recherche Scientifique, UPR 209, Meudon 92195, France

B.D. Padalia

Department of Physics, Indian Institute of Technology, Bombay 400 076, India

R. Vijayaraghavan

Tata Institute of Fundamental Research, Homi Bhabha Road, Bombay 400 005, India

(Received 9 May 1994)

Discovery of a quaternary superconducting system Y-Ni-B-C has been reported recently. Our structural studies on $\text{YNi}_2\text{B}_2\text{C}$ ($T_c \approx 15.5$ K) reveal large and anisotropic thermal vibrations of C atoms in the Y-C plane of the structure. No crystallographic phase transition is observed down to 50 K. Our specific-heat data suggest that $\text{YNi}_2\text{B}_2\text{C}$ is a strong-coupling superconductor. Results of our resistivity, magnetic, and specific-heat data clearly suggest coexistence of superconductivity and magnetism (of Er spins) in $\text{ErNi}_2\text{B}_2\text{C}$ ($T_c \approx 10.5$ K) below ≈ 7 K.

I. INTRODUCTION

The pioneering and seminal discovery of the superconducting alloy system Y-Ni-B-C,^{1,2} the first quaternary superconducting material, came about while attempts were being made to search for superconducting materials containing transition metals other than copper, for example, nickel. The intriguing fact that high- T_c superconductivity is observed only in cuprate systems was the primary motivation to look for such materials. Intermetallics of nickel seemed to be good candidates.

Borides hold out a great promise for interesting physical properties including superconductivity. Therefore nickel-based ternary borides $R\text{Ni}_4\text{B}$ (R = rare earth atoms) were taken up³ for such investigations; they turned out to be rather interesting materials. For example, CeNi_4B (Ref. 4) is strongly Pauli paramagnetic with a linear temperature coefficient of electronic heat capacity, $\gamma \approx 30$ mJ/mol K². SmNi_4B (Ref. 5) is a ferro-

magnet having a rather high magnetic ordering temperature T_M (= 39 K), which is *higher* than T_M (= 36 K) of GdNi_4B .⁵ According to the de Gennes scaling, considering that T_M of GdNi_4B is 36 K, T_M of SmNi_4B should have been ≈ 10 K. Y atoms do not carry a magnetic moment, and in many intermetallics, the magnetic moment of nickel atoms is quenched due to the filling of d holes. For these reasons, YNi_4B was considered to be a good reference material in the above mentioned studies. Its transport and magnetic properties, therefore, were investigated. A sharp and substantial drop of the resistance and diamagnetic response was observed at ≈ 12 K in a sample of nominal composition YNi_4B .¹ Later investigations showed that the superconducting signal got enhanced dramatically upon intentionally adding carbon to YNi_4B during the process of arc melting. Results on two of the C-containing compositions, namely, $\text{YNi}_4\text{BC}_{0.2}$ and $\text{YNi}_2\text{B}_3\text{C}_{0.2}$, were reported² with $T_c \approx 12.5$ K for the former and ≈ 13.5 K for the latter. Besides these

two compositions, several other compositions $\text{YNi}_x\text{B}_y\text{C}_z$ were investigated with their T_c ranging from 12 K to 15 K.⁶ These studies clearly established that superconductivity occurs in the system Y-Ni-B-C with an elevated T_c , $12 \text{ K} \leq T_c \leq 15 \text{ K}$. This work raised the hope that Ni-based systems are possible candidates as intermetallics with high superconducting transition temperature.

Subsequent to our work Cava *et al.* reported superconductivity in $R\text{Ni}_2\text{B}_2\text{C}$ ($R = \text{Y, Lu, Tm, Er, and Ho}$).⁷ Siegrist *et al.*⁸ reported the structure of superconducting phase $\text{LuNi}_2\text{B}_2\text{C}$ ($T_c \approx 16.5 \text{ K}$); it is derived from the ThCr_2Si_2 structure (space group $I4/mmm$) with carbon atoms inserted in the planes of Lu atoms. Here we describe results of our structural, magnetic, and calorimetric measurements on $\text{YNi}_2\text{B}_2\text{C}$ and $\text{ErNi}_2\text{B}_2\text{C}$.

II. EXPERIMENTAL DETAILS

The two compounds $\text{YNi}_2\text{B}_2\text{C}$ and $\text{ErNi}_2\text{B}_2\text{C}$ were prepared by melting high purity elements Y (99.9%), Er (99.9%), Ni (99.9%), B (99.8%), and C (99.7%) in an arc furnace under a protective atmosphere of flowing argon. Samples, sealed in quartz ampoules under vacuum, were annealed at 1050°C for 12 h and cooled to room temperature over a period of 5 h.

Room temperature x-ray diffraction measurements on polycrystalline samples were performed using a Jeol JDX-8030 automatic diffractometer. DIFFRACT-AT software and JCPDS files have been used to check for impurity phases. Low temperature x-ray measurements on $\text{YNi}_2\text{B}_2\text{C}$ were performed using Siemens Kristalloflex diffractometer (Co tube) with a He-TTK low temperature attachment. Structural analysis was carried out on a $\text{YNi}_2\text{B}_2\text{C}$ single crystal ($0.06 \times 0.06 \times 0.015 \text{ mm}^3$) using a Enraf-Nonius four-axis goniometer. Electron diffraction investigations were performed using a transmission electron microscope model No. Jeol 2000FX equipped with an x-ray analyzer (LINK).

The resistivity of the two samples was measured using the standard four-probe technique. The magnetic response as a function of temperature (zero field and field cooled configuration) and as a function of field were studied using a superconducting quantum interference device (SQUID) magnetometer (Quantum Design Inc.). Specific-heat measurements were carried out between 2 K and 25 K in a home-built automated calorimeter using the semiadiabatic heat pulse technique.

III. RESULTS AND DISCUSSIONS

A. Structural considerations

Electron diffraction studies were carried out on samples of $\text{YNi}_2\text{B}_2\text{C}$, prepared by crushing the arc-melted button under CCl_4 in an agate mortar. The diffraction patterns satisfy the constraint $h + k + l = 2n$ and are indexable in terms of a tetragonal system ($a = 3.54 \text{ \AA}$, $c = 10.54 \text{ \AA}$). These observations are consistent with the centered tetragonal structure of the material. The absence of intermediate spots, as compared to those corresponding to the basic structure, rules out the presence of a

superstructure in this system.

Elemental analysis was carried out on the same samples using the LINK x-ray energy analyzer attached to the electron microscope. The major phase of the material had the expected composition. Some occasional regions whose diffraction pattern did not confirm to the tetragonal system were found to contain only Y and Ni. Moreover, regions containing free B and C were never detected.

Structural analysis of a single crystal of $\text{YNi}_2\text{B}_2\text{C}$ was carried out in which 333 x-ray reflections were measured. Out of them, 190 reflections were independent. The centered tetragonal structure of $\text{YNi}_2\text{B}_2\text{C}$, derived from these investigations, is consistent with our electron diffraction results mentioned above and is in agreement with the structure determined by Siegrist *et al.*⁸ $\text{YNi}_2\text{B}_2\text{C}$ belongs to the space group $I4/mmm$. Cell constants determined are $a = 3.526 \text{ \AA}$ and $c = 10.543 \text{ \AA}$ and $Z=2$. The free parameter z , of the position of B atoms, has been refined to be 0.358. Refinement factors are very good ($R = 0.024$ and $R_w = 0.023$). The x-ray diffraction pattern of a polycrystalline sample of $\text{YNi}_2\text{B}_2\text{C}$ essentially shows lines (Fig. 1) that are indexed in terms of the centered tetragonal structure (space group $I4/mmm$), with $a = 3.524(1) \text{ \AA}$ and $c = 10.549(5) \text{ \AA}$.

As shown in Fig. 1, there are a few faint lines that do not belong to this structure. In order to identify the origin of these lines, we carried out an impurity check using the DIFFRAC-AT program, which revealed YB_2C_2 to be the main impurity phase. Both the positions and relative intensities of the impurity lines are indexable in terms of this phase belonging to the space group $P4_2c$. The lattice parameters of the primitive tetragonal structure, $a = 3.784 \text{ \AA}$ and $c = 7.119 \text{ \AA}$, calculated from the position of the impurity lines, are in good agreement with those reported [$a = 3.796 \text{ \AA}$ and $c = 7.124 \text{ \AA}$ (Ref. 9)]. Traces of Ni_3C phase were also inferred to be present. Superconducting phases, such as YB_{12} , YB_6 , and Y_2C_3 , were not detected.

Figure 1 also shows results of calculations of intensities, using the LAZY-PULVERIX program for $\text{YNi}_2\text{B}_2\text{C}$ with atoms distributed in the ThCr_2Si_2 structure as follows: Y at 0,0,0; Ni at 0, 0.5, 0.25; C at 0.5, 0.5, 0; and B at 0, 0, z where $z \approx \frac{3}{8}$. Calculated intensities are in good agreement with the observed ones. The quality of the agreement deteriorates significantly if one does not consider carbon atoms. As B and C atoms are of rather similar size, we considered two other possibilities: (1) exchanging B and C atoms ($\text{YNi}_2\text{C}_2\text{B}$), and (2) putting another C atom at the 0.5, 0, 0 position in the lattice corresponding to the molecular composition $\text{YNi}_2\text{B}_2\text{C}_2$. Accordingly, we prepared samples of nominal composition $\text{YNi}_2\text{C}_2\text{B}$ and $\text{YNi}_2\text{B}_2\text{C}_2$ also, by arc melting under an argon atmosphere. X-ray diffraction of the sample $\text{YNi}_2\text{C}_2\text{B}$ shows that it is multiphase but it does contain the $\text{YNi}_2\text{B}_2\text{C}$ phase. The same is true of $\text{YNi}_2\text{B}_2\text{C}_2$; the sample contains $\text{YNi}_2\text{B}_2\text{C}$ as the major phase; however, the concentration of the impurity phase YB_2C_2 increases significantly. The impurity phase Ni_3B also appears. These considerations establish that C atoms in $\text{YNi}_2\text{B}_2\text{C}$ are located at the vacant site 0.5, 0.5, 0 of the

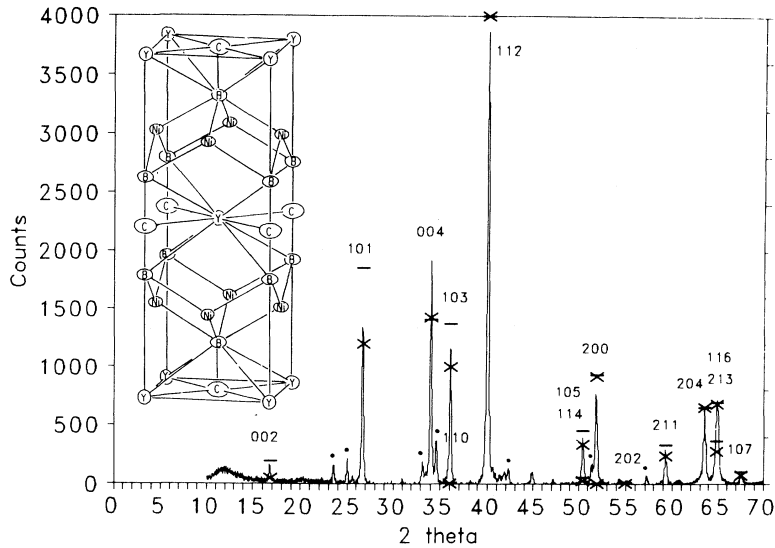


FIG. 1. X-ray diffraction pattern on powdered sample of $\text{YNi}_2\text{B}_2\text{C}$. Lines corresponding to the impurity phase YB_2C_2 are indicated by the symbol (\bullet) above those lines. Results of our intensity calculations (\times) show good agreement with the observed intensities when carbon atoms are assumed to occupy the position (0, 0, 0.5). [Calculated intensity without carbon is shown by the symbol ($-$)]. See the text for further details. Inset shows the structure of $\text{YNi}_2\text{B}_2\text{C}$ determined from single-crystal diffraction studies. Ellipsoids of thermal vibrations of various atoms as deduced from ORTEP software are shown. Note the rather large thermal amplitude of C atoms in the Y-C plane. Isotropic thermal parameters, deduced from these measurements, are 0.34 \AA^2 , 0.30 \AA^2 , 0.37 \AA^2 , and 0.70 \AA^2 for Y, Ni, B, and C atoms, respectively.

ThCr_2Si_2 structure.

It is instructive to compare the lattice constants of $\text{YNi}_2\text{B}_2\text{C}$ with those of several related materials of ThCr_2Si_2 structure: YM_2Si_2 ($M = \text{Fe, Co, Ni}$); YM_2B_2 ($M = \text{Fe, Co}$) (see Table I). The lattice constant a among the first three materials and also among the latter two materials changes only slightly. The c parameter, however, varies considerably and is minimum for YCo_2B_2 . One possible reason why YNi_2B_2 does not form (this work) is that, considering the variation of the parameters of the materials YM_2B_2 ($M = \text{Fe, Co}$), value of c of the hypothetical YNi_2B_2 would have been much smaller ($\approx 9.3 \text{ \AA}$) which, perhaps, falls outside the limit of stability of the ThCr_2Si_2 structure. In fact, most known materials of ThCr_2Si_2 have $c > 9.3 \text{ \AA}$. Introduction of C atoms expands the c axis (it is the largest among those shown in Table I) and helps stabilize the ThCr_2Si_2 structure. Expansion of the c parameter takes place as the C atoms in the R plane push away B and Ni planes. There is a slight shortening of the a axis [compare the a parameter, Table I, of $\text{YNi}_2\text{B}_2\text{C}$ with those of YM_2B_2 ($M = \text{Fe, Co}$)] which may be due to the strong bonding of C atoms with R atoms. Both these effects lead to enhanced anisotropy of the $\text{YNi}_2\text{B}_2\text{C}$ tetragonal structure.

We also prepared the materials $\text{RNi}_2\text{B}_2\text{C}$ ($R = \text{Ho, Er, Tm}$) which have also been recently shown^{7,8} to crystallize in the $\text{YNi}_2\text{B}_2\text{C}$ structure. Their lattice parameters a and c , respectively, are for $\text{HoNi}_2\text{B}_2\text{C}$, $3.513(1) \text{ \AA}$, $10.525(3) \text{ \AA}$; for $\text{ErNi}_2\text{B}_2\text{C}$, $3.503(1) \text{ \AA}$ and $10.560(5) \text{ \AA}$; and for $\text{TmNi}_2\text{B}_2\text{C}$, $3.485(1) \text{ \AA}$, $10.591(3) \text{ \AA}$. It is to be noted that while the cell constant a does exhibit the usual lanthanide contraction, the cell parameter c expands instead.

Thermal vibrations of various atoms were deduced from the diffraction data using ORTEP software. C atoms have a rather large amplitude of thermal vibration, especially in the (Y-C) plane [Fig. 1 (inset)], as compared to that of Y, Ni, and B atoms. Small displacements of C atoms from their theoretical position and/or off-stoichiometry of the material also may give rise to the

effects in x-ray diffraction that are interpretable as arising due to large thermal vibrations. In this context, it must be pointed out that the refinement factor is rather good.

We have also carried out x-ray diffraction measurements on $\text{YNi}_2\text{B}_2\text{C}$ at 50 K, the lowest temperature that we could achieve in our equipment. No crystallographic transition occurs in the temperature range 300–50 K. The lattice parameters obtained at 50 K are $a = 3.521(1) \text{ \AA}$ and $c = 10.549(4) \text{ \AA}$. There is essentially no change in the Ni-B distance ($= 2.102 \text{ \AA}$), which means that the Ni_2B_2 framework is rigid. The Y-B distance ($= 2.905 \text{ \AA}$ at 300 K) decreases by 0.003 \AA as the sample is cooled from 300 K to 50 K. However, the C-B distance ($= 1.496$

TABLE I. Lattice constants a (\AA) and c (\AA) of $\text{YNi}_2\text{B}_2\text{C}$ and a number of materials that are structurally related to it.

Material	a (\AA)	c (\AA)
YFe_2Si_2	3.920	$9.920^{\text{a,b}}$
YCo_2Si_2	3.892	9.759^{a}
YNi_2Si_2	3.950	9.530^{c}
YFe_2B_2	3.546	9.555^{d}
YCo_2B_2	3.56	9.358^{e}
YNi_2B_2		does not form ^f
$\text{YNi}_2\text{B}_2\text{C}$	3.53	10.57 (300 K) ^g
	$3.524(1)$	$10.545(5)$ (300 K) ^f
	$3.521(1)$	$10.549(5)$ (50 K) ^f

^aD. Rossi, R. Marazza, and R. Ferro, *J. Less Common. Met.* **58**, 203 (1978).

^bO. I. Bodak *et al.*, *Izv. Akad. Nauk. USSR Neorg. Mater.* **7**, 41 (1971) [*Inorg. Mater. (USSR)*].

^cW. Rieger and E. Parthe, *Monatsh. Chem.* **100**, 444 (1969).

^dG.F. Stpanchikova, Yu. B. Ku'zma, and B.I. Chernjak, *Dopov. Akad. Nauk Ukr. RSR, Ser. A* **10**, 951 (1978).

^eK. Nihara, T. Shishido, and S. Yajima, *Bull. Chem. Soc. Jpn.* **46**, 1137 (1973).

^fThis work.

^gReference 8.

Å at 300 K) increases by 0.0025 Å and the B-B distance (2.983 Å at 300 K) also increases by 0.005 Å.

B. Resistivity measurements

Figure 2 shows the typical results of the resistivity measurements of $\text{YNi}_2\text{B}_2\text{C}$ and $\text{ErNi}_2\text{B}_2\text{C}$. Several features of these measurements must be pointed out:

(i) The resistive transition, $T_c = 15.3$ K in $\text{YNi}_2\text{B}_2\text{C}$, and 10.3 K in $\text{ErNi}_2\text{B}_2\text{C}$, is sharp. The width of the transition (90%–10% resistivity) is ≈ 0.5 K.

(ii) The magnitude of the room temperature resistivity is large ($>100 \mu\Omega$) for a metallic system. This implies that the electron-phonon interaction may be rather large. The resistivity decreases linearly with temperature, down to 60 K in $\text{YNi}_2\text{B}_2\text{C}$ and down to 50 K in $\text{ErNi}_2\text{B}_2\text{C}$.

(iii) It is noteworthy that the resistance of $\text{ErNi}_2\text{B}_2\text{C}$, if extrapolated linearly from the high temperature side, passes through the origin. This is observed in many high- T_c superconductors.

(iv) The resistivity of $\text{ErNi}_2\text{B}_2\text{C}$ is higher than the resistivity in $\text{YNi}_2\text{B}_2\text{C}$. Magnetic scattering of the carriers due to Er spins is responsible for this.

We wish to point out that in the measurements carried out on different samples of these materials, there are variations in the absolute values of the resistivity and its temperature coefficient. However, all the samples showed the features mentioned above. These materials are highly crystalline with preferential orientation of crystallites in the polycrystal material. We believe that these features may be responsible for the observed variation from sample to sample.

High- T_c cuprate materials, with T_c as low as 10 K, exhibit a linear temperature dependence of resistivity down to their T_c . Scattering of the carriers from two-dimensional (2D) antiferromagnetic fluctuations of Cu spins has been suggested to be one possible mechanism of this behavior.¹⁰ It is not clear to us, at present, if such a mechanism is operative in these material as well, considering highly two-dimensional nature of their crystal structure. If so, it would imply that moments on Ni atoms are not zero identically and that they are both spatially and

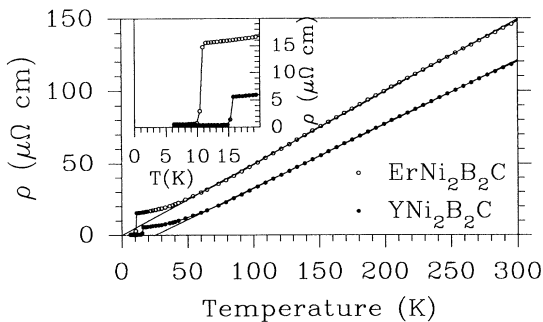


FIG. 2. Temperature dependence of resistivity (ρ in $\mu\Omega$ cm) of $\text{YNi}_2\text{B}_2\text{C}$ and $\text{ErNi}_2\text{B}_2\text{C}$. It is to be noted that the extrapolated $\rho(T)$ in the case of $\text{ErNi}_2\text{B}_2\text{C}$ passes through the origin. The inset shows the resistivity near the superconducting transition temperatures in the two samples.

temporally correlated. More extensive efforts are needed to clarify such a basic and important question as this will have bearing on the mechanism of Cooper pairing in quaternary borocarbides. Recent muon spin resonance (μSR) experiments on $\text{LuNi}_2\text{B}_2\text{C}$ and $\text{TmNi}_2\text{B}_2\text{C}$ suggest that Ni ions do carry a moment, which are inferred to undergo a magnetic ordering below ≈ 1.4 K.¹¹

C. Magnetic susceptibility and magnetization measurements

Figure 3 shows the magnetic susceptibility as function of temperature of both the samples in their normal state. The inverse susceptibility $\chi(T)^{-1}$ of $\text{ErNi}_2\text{B}_2\text{C}$ as a function of temperature is also shown in Fig. 3.

The observed susceptibility $\chi(T)$ of $\text{YNi}_2\text{B}_2\text{C}$ is temperature dependent, suggesting thereby that the material is not a Pauli paramagnet. $\chi(T)$ was fit to $\chi(T) = \chi(0) + C/(T + \Theta_p)$ in the temperature range 15–300 K. From this fit, μ_{eff} per Ni atom was obtained to be $0.18\mu_B$ and Θ_p to be +54 K. The contribution to the susceptibility from the impurity phases may alter these values. It may be pointed out that, as mentioned earlier, μSR experiments¹¹ do detect a moment on Ni atoms in $\text{LuNi}_2\text{B}_2\text{C}$.

The inverse susceptibility $\chi(T)^{-1}$ of $\text{ErNi}_2\text{B}_2\text{C}$ varies linearly with temperature, suggesting a Curie-Weiss (CW) behavior of $\chi(T) [= C/(T + \Theta_p)]$. $\mu_{\text{eff}} = 9.32\mu_B$ per formula unit and $\Theta_p \approx -2$ K were derived from this fit. It is to be noted that μ_{eff} is less than that of the Er^{3+} free ion ($9.59\mu_B$). One possibility for the reduced magnetic moment is that Er and Ni moments are strongly antiferromagnetically correlated in the paramagnetic state. It should be of interest to investigate these and other related aspects by neutron diffraction measurements.

Figure 4 shows the superconducting diamagnetic response of the field-cooled (FC) and the zero-field-cooled (ZFC) samples of $\text{YNi}_2\text{B}_2\text{C}$ in a magnetic field of 30 G as a function of temperature. It can be seen from the figure

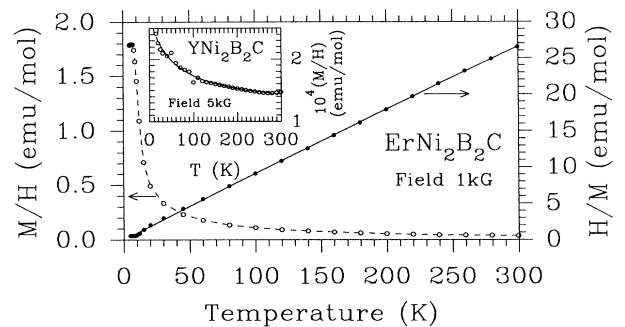


FIG. 3. Temperature dependence of magnetic susceptibility of the paramagnetic state in an applied field of 5 kG for $\text{YNi}_2\text{B}_2\text{C}$ (see the inset; the line is a fit to a CW behavior) and 1 kG for $\text{ErNi}_2\text{B}_2\text{C}$. The figure does not show the diamagnetic response due to superconductivity (i) $\text{ErNi}_2\text{B}_2\text{C}$ as the sample is field cooled (ii) in $\text{YNi}_2\text{B}_2\text{C}$ because the data points are limited to $T > T_c$. Solid circles show the inverse of susceptibility in $\text{ErNi}_2\text{B}_2\text{C}$. The line passing through the solid circles is a Curie-Weiss fit.

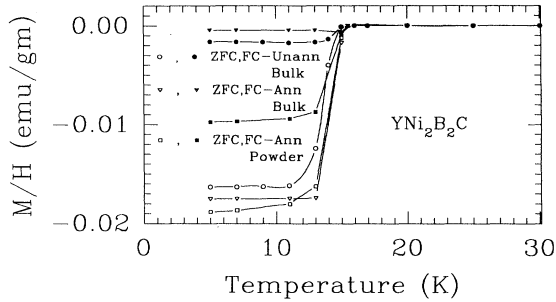


FIG. 4. Temperature dependence of diamagnetic response of $\text{YNi}_2\text{B}_2\text{C}$ [unannealed bulk, annealed bulk, and powder of the annealed sample at a field of 30 G both in zero-field-cooled (ZFC) and field-cooled (FC) conditions]. The shielding signal (zero field cooled) is very close to 100% of the perfect diamagnetism. The figure also shows the effect of annealing on the diamagnetic response of the material.

that a nearly 100% (of the ideal diamagnetism) shielding signal is observed in the as-cast and annealed solid samples and the powder of the annealed sample of $\text{YNi}_2\text{B}_2\text{C}$. The annealed solid sample shows a very small Meissner signal (close to zero). However, the powder of the annealed sample shows the best ($\approx 50\%$) Meissner signal. The significant difference between the Meissner signals of the annealed solid and the powder samples may be because of a reduction in field trapping due to an enhanced surface to volume ratio on powdering. That the Meissner signal is less than the ideal value may be due to the possible low value (< 30 G) of the lower critical field H_{c1} and also due to possible crystalline imperfections.

The magnetization $M(H)$ of $\text{YNi}_2\text{B}_2\text{C}$, as a function of applied field H with $0 < H < 55$ kG, has been measured at various temperatures $5 \text{ K} < T < 20$ K. The results are typical of a type-II superconductor (Fig. 5). Considering that $H_{c1}(T)$ is the field at which $M(H, T)$ deviates from linearity, we estimate, from Fig. 5, $H_{c1}(T) \approx 30$ G at 5 K. A more detailed study of the magnetic response of this material is presented in Ref. 12 in which the material has been examined following various sequences of applied magnetic field and temperature.

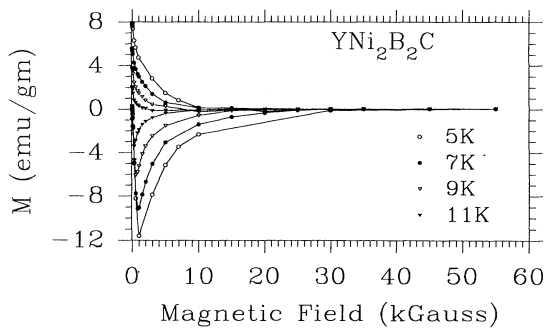


FIG. 5. Magnetization versus field at various temperatures, for both increasing and decreasing fields, in $\text{YNi}_2\text{B}_2\text{C}$. Each run starts with a zero-field-cooled condition. The value of upper critical field H_{c2} has been estimated from these measurements. The line is a guide to the eye [see Fig. 6 for $H_{c2}(T)$].

We have determined the variation of $H_{c2}(T)$ with temperature from magnetoresistance measurements.¹³ The results of these measurements are shown in Fig. 6. H_{c2} at 5 K is ≈ 4.5 T. It should be noted that our data suggest that the temperature dependence of $H_{c2}(T)$ (Fig. 6) is different from that of conventional type-II superconductors (inset, Fig. 6). The slope $dH_{c2}(T)/dT$ is close to zero at T_c and increases with a decrease of temperature in $\text{YNi}_2\text{B}_2\text{C}$, whereas in a conventional type-II superconductor $dH_{c2}(T)/dT$ is nonzero at T_c and is nearly constant for a considerable range of temperature below T_c (see the inset of Fig. 6). This feature, which points to an unconventional nature of superconductivity in $\text{YNi}_2\text{B}_2\text{C}$, deserves to be investigated further. With $\xi(T) = \Phi_0/(2\pi H_{c2}(T))$, we estimate a value of the coherence length of $\xi \approx 80$ Å at 5 K.

The superconducting diamagnetic response of $\text{ErNi}_2\text{B}_2\text{C}$ in as-cast solid and powdered samples is shown in Fig. 7. The solid sample exhibits a shielding signal, in the ZFC configuration, which is quite close to that of perfect diamagnetism. The powdered sample also shows a good shielding signal ($\approx 50\%$ of ideal diamagnetism). However, noteworthy is the fact that in both the cases, in the field-cooled configuration, the material exhibits a positive response down to the lowest temperature. This is an indication of sufficient field penetration, even at a field of 30 G, and field trapping. The paramagnetic contribution of Er spins in the flux lines in the interior of the material masks the superconducting diamagnetic response of the material.

There is a small anomaly in the magnetic response of $\text{ErNi}_2\text{B}_2\text{C}$, in the FC configuration, in the neighborhood of 7 K. We associate this with a magnetic ordering of Er spins around 7 K (see results below of heat capacity measurements also). In the zero-field-cooled state, diamagnetism due to superconductivity shields the signal due to magnetic order. Thus, a magnetically ordered state of Er spins coexists with superconductivity in this system. Figure 8 shows the field dependence of $M(H)$ at 5 K in $\text{ErNi}_2\text{B}_2\text{C}$. It crosses zero at a low field of ≈ 400 G. The magnetism due to Er spins dominates the magnetic response of the material above this field.

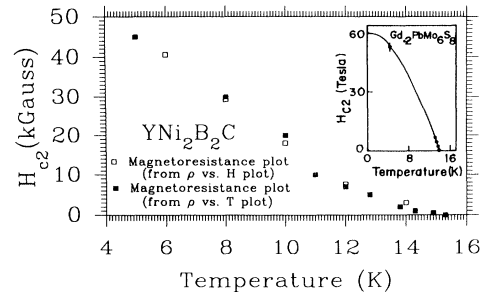


FIG. 6. Temperature dependence of $H_{c2}(T)$ in $\text{YNi}_2\text{B}_2\text{C}$ obtained from magnetoresistance measurements (Ref. 13). Solid squares are values of H_{c2} obtained from ρ vs T data at various fields and open squares are values of H_{c2} obtained from ρ vs H data at various temperatures. The inset shows the temperature dependence of $H_{c2}(T)$ in a conventional type-II superconductor $\text{Gd}_{0.2}\text{PbMo}_6\text{S}_8$ (see Ref. 14, p. 26).

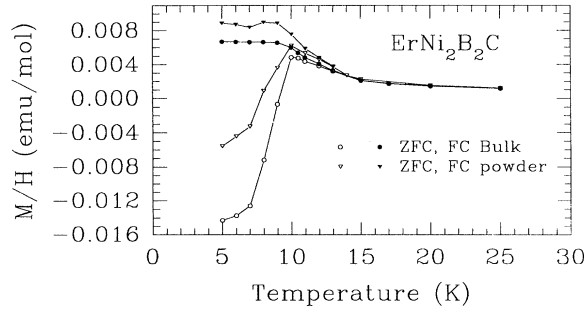


FIG. 7. Superconducting diamagnetic response in solid and powdered samples of $\text{ErNi}_2\text{B}_2\text{C}$. See text.

D. Heat capacity measurements

Figure 9 shows the molar heat capacity C_p/T of an annealed sample of $\text{YNi}_2\text{B}_2\text{C}$ plotted as a function of T^2 in the temperature range $5 \text{ K} < T < 22 \text{ K}$. The heat capacity of the as-cast sample of $\text{YNi}_2\text{B}_2\text{C}$ was also measured. We find that the anomaly in C_p due to superconductivity is narrower, and occurs at a higher temperature in the annealed sample, suggesting that the quality of the sample improves on annealing. This is reflected in the x-ray diffraction pattern of the material as well and also in its diamagnetic response.

The data points above the superconducting transition temperature were fit to the expression $C_p/T = \gamma + \beta T^2 + \delta T^4$, where γ and β are the coefficients of the electronic and the lattice heat capacities, respectively. The third term δ was added as the C_p/T plot above the transition temperature has a slight curvature. The results of the fit are $\gamma = 8.9 \text{ mJ/mol K}^2$, $\beta = 0.163 \text{ mJ/mol K}^4$, and $\delta = 2.37 \times 10^{-5} \text{ mJ/mol K}^6$. We obtain a value of the Debye temperature $\Theta_D = 415 \text{ K}$ from the value of β . Assuming an idealized superconducting transition at the midpoint ($T^2 = 210 \text{ K}^2$) of the specific-heat anomaly, we get $\Delta C_p/\gamma T_c = 3.6$. This is much higher than 1.43, the BCS value for the weak-coupling limit. Movshovich *et al.*¹⁵ report a value of $\gamma = 18.7 \text{ mJ/mol K}^2$ measured using a single crystal of $\text{YNi}_2\text{B}_2\text{C}$. We do not understand the reason for this difference; γ should be in-

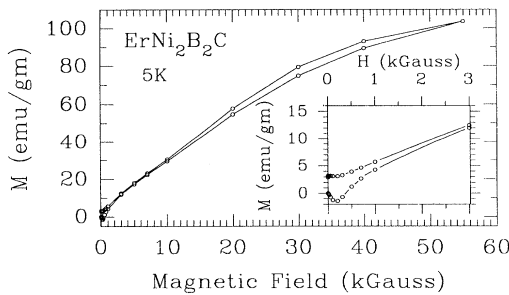


FIG. 8. Magnetization versus field at 5 K, for both increasing and decreasing fields, in $\text{ErNi}_2\text{B}_2\text{C}$. The run starts with a zero-field-cooled condition. The inset shows an expanded view of the isothermal magnetisation curve near the low magnetic field region.

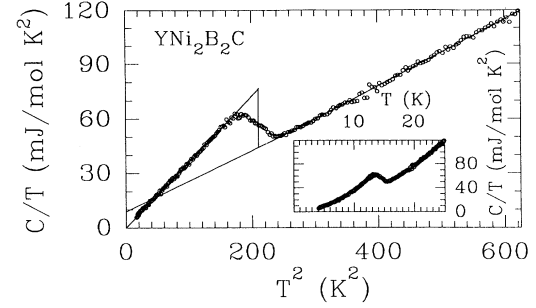


FIG. 9. Temperature coefficient of heat capacity C_p/T of $\text{YNi}_2\text{B}_2\text{C}$ as a function of T^2 . The inset shows C_p/T as a function of T . Data in the temperature interval $16 \text{ K} < T < 22 \text{ K}$ have been fit to the expression $C_p/T = \gamma + \beta T^2 + \delta T^4$. The values of the fitting parameters are given in the text. Data below T_c , after making the phonon contribution, are fit to the expression $C_p/T = 0.363 T^2$. Inset shows the C_p/T vs T plot.

dependent of whether the material is polycrystalline or a single crystal. It is interesting to point out that the values of T_c and Θ_D are very similar to those of PbMo_6S_8 ,¹⁴ which is considered to be a strong-coupling superconductor. This suggests that strong-coupling effects are operative in $\text{YNi}_2\text{B}_2\text{C}$. The large value of the ratio T_c/Θ_D is also consistent with this conclusion.¹⁴ We wonder if the large vibrations of C atoms in this system play any role in the strong electron-phonon coupling.

The heat capacity of $\text{YNi}_2\text{B}_2\text{C}$, below the superconducting transition down to 5 K, follows a linear C_p/T vs T^2 relationship. It should be of interest to extend these measurements, below 5 K, to check and confirm this temperature dependence of C_p . It may be pointed out that the power-law behavior of the heat capacity in the superconducting state of heavy fermion systems has been taken as an indication of unconventional superconductivity where the symmetry of the superconducting energy gap is lower than the symmetry of the Fermi surface.¹⁶

The C_p/T vs T^2 plot for $\text{ErNi}_2\text{B}_2\text{C}$ is shown in Fig. 10.

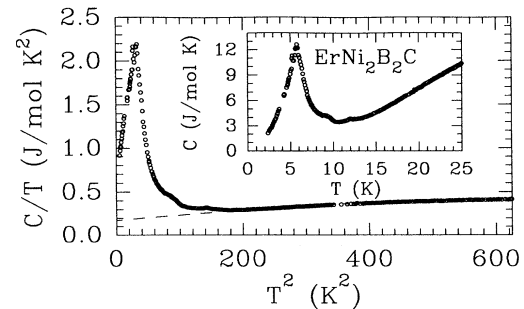


FIG. 10. C_p/T of $\text{ErNi}_2\text{B}_2\text{C}$ as a function of T^2 . The inset shows C_p/T as a function of T . The large anomaly at $\approx 6.5 \text{ K}$ indicates a magnetic transition of Er spins. The large γ (indicated by the dashed line, following the fit $C_p/T = 176.4 + 0.68 T^2 + 4.8 \times 10^{-4} T^4$ in the temperature range 14–25 K) is due to crystal field effects. The inset shows the C_p vs T plot showing the jump in C_p at the magnetic ordering temperature.

The inset of the figure shows C_p/T vs T . A large anomaly is observed with the peak of heat capacity occurring around 5.8 K. We interpret this as due to the magnetic ordering of Er spins. Since the resistivity does not show any reentrant behavior below this temperature, and the material continues to exhibit a diamagnetic response down to 5 K, we conclude that superconductivity and magnetic ordering coexist below ≈ 7 K in this system.

The coexistence of superconductivity and magnetic ordering occurs, for example, in ternary rare earth rhodium borides¹⁷ and molybdenum chalcogenides¹⁷ and high- T_c superconductors. It is to be recalled that in the ternary system ErRh_4B_4 ($T_c = 8.2$ K), a reentrant transition to the normal state is observed below the magnetic ordering temperature ($=1.2$ K). This is because in ErRh_4B_4 , Er spins undergo a ferromagnetic ordering¹⁸ and superconductivity is destroyed below the magnetic ordering temperature. On the other hand, in cases like TmRh_4B_4 ,¹⁹ where Tm ions are known to order antiferromagnetically, superconductivity is not destroyed due to magnetic ordering. These results suggest that it is very likely that Er spins in $\text{ErNi}_2\text{B}_2\text{C}$ order antiferromagnetically near 6 K.

The heat capacity anomaly ($\Delta C_p \approx 500$ mJ/mol K) at the superconducting transition in $\text{ErNi}_2\text{B}_2\text{C}$ is seen as a structure at ≈ 10.2 K. A small bump in the heat capacity near 12 K is possibly due to some minor impurity phase. The C_p/T vs T^2 plot of $\text{ErNi}_2\text{B}_2\text{C}$ is linear above 180 K² and an extrapolation to $T=0$ K gives a C_p/T value of 225 mJ/mol K². This large value of $(C_p/T)_{T=0}$, cannot be attributed to the itinerant degrees of freedom as the specific-heat jump at the superconducting temperature is too small to be consistent with this value of $(C_p/T)_{T=0}$. It is conceivable that the large value of

C_p above 10 K arises due to crystal field effects. Just as $\text{YNi}_2\text{B}_2\text{C}$, $\text{ErNi}_2\text{B}_2\text{C}$ also should be a strong-coupling superconductor. However, due to the reasons mentioned above, it is not possible to obtain a reliable estimate of γ corresponding to the itinerant degrees of freedom. Therefore it is difficult to comment upon the strength of the electron-phonon coupling in this system.

IV. CONCLUSION AND SUMMARY

To summarize, we have carried out detailed structural investigations in $\text{YNi}_2\text{B}_2\text{C}$ ($T_c = 15.5$ K). Our results show that there is no superstructure in this system. Carbon atoms have a large amplitude of thermal vibrations in the Y-C plane. The material does not undergo any crystallographic transition down to 50 K. $\text{YNi}_2\text{B}_2\text{C}$ has a high upper critical field $H_{c2} \approx 50$ kG at 5 K. The temperature dependence of H_{c2} in these materials is rather different from that observed in conventional type-II superconductors. The large values of $\Delta C_p/\gamma T_c$ and T_c/Θ_D suggest strong-coupling effects to be operative in this material. The power-law T dependence of C_p below T_c suggests that the superconducting energy gap parameter has zeros on the Fermi surface. More detailed studies are required to establish the unconventional nature of superconductivity in this system. Superconductivity and (anti)ferromagnetic ordering coexist in $\text{ErNi}_2\text{B}_2\text{C}$ below the magnetic ordering temperature (≈ 7 K).

Note added in proof. Recently, neutron-diffraction studies on $\text{ErNi}_2\text{B}_2\text{C}$ have confirmed antiferromagnetic ordering of Er and Ni moments. See, S. K. Sinha, J. W. Lynn, T. E. Grigreit, Z. Hossain, L. C. Gupta, R. Nagarajan and C. Godart, Phys. Rev. B **51**, 681 (1995).

*C. Godart and C. Levy-Clement were at TIFR (Bombay) while this work was being carried out.

¹Chandan Mazumdar, R. Nagarajan, C. Godart, L.C. Gupta, M. Latroche, S.K. Dhar, C. Levy-Clement, B.D. Padalia, and R. Vijayaraghavan, Solid State Commun. **87**, 413 (1993).

²R. Nagarajan, Chandan Mazumdar, Zakir Hossain, S.K. Dhar, K.V. Gopalakrishnan, L.C. Gupta, C. Godart, B.D. Padalia, and R. Vijayaraghavan, Phys. Rev. Lett. **72**, 274 (1994).

³Chandan Mazumdar, R. Nagarajan, L.C. Gupta, B.D. Padalia, and R. Vijayaraghavan, Proc. Solid State Phys. Symposium, Dept. Atomic Energy, India, Vol. 33C, 265 (1991).

⁴Chandan Mazumdar, R. Nagarajan, S.K. Dhar, L.C. Gupta, B.D. Padalia, and R. Vijayaraghavan, Proc. Solid State Phys. Symposium, Dept. Atomic Energy, India, Vol. 34C, 241 (1991).

⁵Chandan Mazumdar, R. Nagarajan, L.C. Gupta, B.D. Padalia, and R. Vijayaraghavan (unpublished).

⁶Unpublished results of Ref. 2.

⁷R.J. Cava, H. Takagi, B. Batlogg, H.W. Zandbergen, J.J. Krajewski, W.F. Peck, R.B. van Dover, R.J. Felder, T. Siegrist, K. Mizuhashi, J.O. Lee, H. Eisaki, S.A. Carter, and S. Uchida, Nature **367**, 252 (1994).

⁸T. Siegrist, H.W. Zandbergen, R.J. Cava, J.J. Krajewski, and W.F. Peck, Nature **367**, 254 (1994).

⁹J. Bauer and O. Bars, Acta Crystallogr. B **36**, 1540 (1980).

¹⁰Y. Iye, J. Phys. Chem. Solids, **53**, 1561 (1992) and references therein. See also T. Moriya, Y. Takahashi, and K. Ueda, J. Phys. Soc. Jpn. **59**, 2905 (1990); H. Kohno and Y. Yamada, Prog. Theor. Phys. **85**, 13 (1991).

¹¹D.W. Cooke, J.L. Smith, S.F.J. Cox, A. Morrobel-Sosa, R.L. Lichti, T.L. Estle, B. Hitti, L.C. Gupta, R. Nagarajan, Z. Hossain, C. Mazumdar, and C. Godart (unpublished).

¹²S.B. Roy, Zakir Hossain, A.K. Pradhan, Chandan Mazumdar, P. Chaddah, R. Nagarajan, L.C. Gupta, and C. Godart, Physica C **228**, 319 (1994).

¹³Chandan Mazumdar and A. K. Nigam (private communication).

¹⁴See, for example, Gerald Burns, in *High-Temperature Superconductivity: An Introduction* (Academic, Boston, 1992), and references therein.

¹⁵R. Movshovich, M.F. Hundley, J.D. Thompson, P.C. Canfield, B.K. Cho, and A.V. Chubukov, Physica C **227**, 381 (1994).

¹⁶James F. Annett, Nigel Goldenfeld, and S.R. Renn, in *Physical Properties of High Temperature Superconductors II*, edited by D.M. Ginsberg (World Scientific, Singapore, 1990), p. 571; see also Peter Fulde, Joachim Keller, and

Gertrud Zwicknagl, in *Solid State Physics*, edited by Henry Ehrenreich and David Turnbull (Academic, New York, 1988), Vol. 41, p. 2.

¹⁷See various papers in *Superconductivity in Ternary Compounds I,II*, Topics in Current Physics, Vols. 32 and 34, edited by Ø. Fisher and M.B. Maple (Springer-Verlag, Berlin, 1982).

¹⁸B.T. Matthias, E. Corenzwit, J.M. Vandenberg, and H.E. Barz, Proc. Natl. Acad. Sci. USA, **74**, 1334 (1977); W.A.

Fertig, D.C. Johnston, L.E. DeLong, R.W. McCallum, M.B. Maple, and B.T. Matthias, Phys. Rev. Lett. **38**, 387 (1977); D.E. Moncton, D.B. McWhan, J. Eckert, G. Shirane, and W. Thomlinson, *ibid.* **39**, 1164 (1977).

¹⁹B.T. Matthias, E. Corenzwit, J.M. Vandenberg, and H.E. Barz, Proc. Natl. Acad. Sci. USA **74**, 1334 (1977); H.C. Hamaker, H.B. MacKay, M.S. Torikachvili, L.D. Woolf, M.B. Maple, W. Odoni, and H.R. Ott, J. Low Temp. Phys. **44**, 553 (1981).